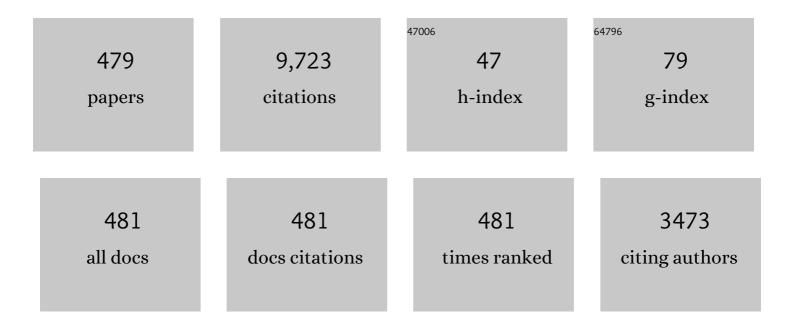
List of Publications by Year in descending order

Source: https://exaly.com/author-pdf/6947933/publications.pdf Version: 2024-02-01



#	Article	IF	CITATIONS
1	Tutorial on Remote Sensing Using GNSS Bistatic Radar of Opportunity. IEEE Geoscience and Remote Sensing Magazine, 2014, 2, 8-45.	9.6	388
2	SMOS: The Challenging Sea Surface Salinity Measurement From Space. Proceedings of the IEEE, 2010, 98, 649-665.	21.3	339
3	Downscaling SMOS-Derived Soil Moisture Using MODIS Visible/Infrared Data. IEEE Transactions on Geoscience and Remote Sensing, 2011, 49, 3156-3166.	6.3	328
4	The visibility function in interferometric aperture synthesis radiometry. IEEE Transactions on Geoscience and Remote Sensing, 2004, 42, 1677-1682.	6.3	262
5	Sensitivity of GNSS-R Spaceborne Observations to Soil Moisture and Vegetation. IEEE Journal of Selected Topics in Applied Earth Observations and Remote Sensing, 2016, 9, 4730-4742.	4.9	208
6	Soil Moisture Retrieval Using GNSS-R Techniques: Experimental Results Over a Bare Soil Field. IEEE Transactions on Geoscience and Remote Sensing, 2009, 47, 3616-3624.	6.3	184
7	Land Geophysical Parameters Retrieval Using the Interference Pattern GNSS-R Technique. IEEE Transactions on Geoscience and Remote Sensing, 2011, 49, 71-84.	6.3	177
8	A Downscaling Approach for SMOS Land Observations: Evaluation of High-Resolution Soil Moisture Maps Over the Iberian Peninsula. IEEE Journal of Selected Topics in Applied Earth Observations and Remote Sensing, 2014, 7, 3845-3857.	4.9	146
9	The determination of surface salinity with the European SMOS space mission. IEEE Transactions on Geoscience and Remote Sensing, 2004, 42, 2196-2205.	6.3	140
10	The processing of hexagonally sampled signals with standard rectangular techniques: application to 2-D large aperture synthesis interferometric radiometers. IEEE Transactions on Geoscience and Remote Sensing, 1997, 35, 183-190.	6.3	138
11	A Change Detection Algorithm for Retrieving High-Resolution Soil Moisture From SMAP Radar and Radiometer Observations. IEEE Transactions on Geoscience and Remote Sensing, 2009, 47, 4125-4131.	6.3	136
12	The WISE 2000 and 2001 field experiments in support of the SMOS mission: sea surface L-band brightness temperature observations and their application to sea surface salinity retrieval. IEEE Transactions on Geoscience and Remote Sensing, 2004, 42, 804-823.	6.3	132
13	Consolidating the Precision of Interferometric GNSS-R Ocean Altimetry Using Airborne Experimental Data. IEEE Transactions on Geoscience and Remote Sensing, 2014, 52, 4992-5004.	6.3	130
14	Sea Ice Detection Using U.K. TDS-1 GNSS-R Data. IEEE Transactions on Geoscience and Remote Sensing, 2017, 55, 4989-5001.	6.3	130
15	Combining SMOS with visible and near/shortwave/thermal infrared satellite data for high resolution soil moisture estimates. Journal of Hydrology, 2014, 516, 273-283.	5.4	113
16	Radiometric sensitivity computation in aperture synthesis interferometric radiometry. IEEE Transactions on Geoscience and Remote Sensing, 1998, 36, 680-685.	6.3	105
17	GEROS-ISS: GNSS REflectometry, Radio Occultation, and Scatterometry Onboard the International Space Station. IEEE Journal of Selected Topics in Applied Earth Observations and Remote Sensing, 2016, 9, 4552-4581.	4.9	99
18	MIRAS end-to-end calibration: application to SMOS L1 processor. IEEE Transactions on Geoscience and Remote Sensing, 2005, 43, 1126-1134.	6.3	91

#	Article	IF	CITATIONS
19	Airborne GNSS-R Wind Retrievals Using Delay–Doppler Maps. IEEE Transactions on Geoscience and Remote Sensing, 2013, 51, 626-641.	6.3	85
20	Retrieval of Significant Wave Height and Mean Sea Surface Level Using the GNSS-R Interference Pattern Technique: Results From a Three-Month Field Campaign. IEEE Transactions on Geoscience and Remote Sensing, 2015, 53, 3198-3209.	6.3	84
21	An Efficient Algorithm to the Simulation of Delay–Doppler Maps of Reflected Global Navigation Satellite System Signals. IEEE Transactions on Geoscience and Remote Sensing, 2009, 47, 2733-2740.	6.3	82
22	Altimetry with GNSS-R interferometry: first proof of concept experiment. GPS Solutions, 2012, 16, 231-241.	4.3	81
23	Correction of the Sea State Impact in the L-Band Brightness Temperature by Means of Delay-Doppler Maps of Global Navigation Satellite Signals Reflected Over the Sea Surface. IEEE Transactions on Geoscience and Remote Sensing, 2008, 46, 2914-2923.	6.3	79
24	On-board phase and modulus calibration of large aperture synthesis radiometers: study applied to MIRAS. IEEE Transactions on Geoscience and Remote Sensing, 1996, 34, 1000-1009.	6.3	72
25	The emissivity of foam-covered water surface at L-band: theoretical modeling and experimental results from the FROG 2003 field experiment. IEEE Transactions on Geoscience and Remote Sensing, 2005, 43, 925-937.	6.3	72
26	Using GNSS-R Imaging of the Ocean Surface for Oil Slick Detection. IEEE Journal of Selected Topics in Applied Earth Observations and Remote Sensing, 2013, 6, 217-223.	4.9	72
27	Review of crop growth and soil moisture monitoring from a groundâ€based instrument implementing the Interference Pattern GNSSâ€R Technique. Radio Science, 2011, 46, .	1.6	71
28	L-band vegetation optical depth seasonal metrics for crop yield assessment. Remote Sensing of Environment, 2018, 212, 249-259.	11.0	69
29	Spatial Resolution in GNSS-R Under Coherent Scattering. IEEE Geoscience and Remote Sensing Letters, 2020, 17, 32-36.	3.1	67
30	Microwave interferometric radiometry in remote sensing: An invited historical review. Radio Science, 2014, 49, 415-449.	1.6	66
31	Sensitivity of TDS-1 GNSS-R Reflectivity to Soil Moisture: Global and Regional Differences and Impact of Different Spatial Scales. Remote Sensing, 2018, 10, 1856.	4.0	66
32	Synthesis of large low-redundancy linear arrays. IEEE Transactions on Antennas and Propagation, 2001, 49, 1881-1883.	5.1	63
33	A new empirical model of sea surface microwave emissivity for salinity remote sensing. Geophysical Research Letters, 2004, 31, .	4.0	63
34	Improved Image Reconstruction Algorithms for Aperture Synthesis Radiometers. IEEE Transactions on Geoscience and Remote Sensing, 2008, 46, 146-158.	6.3	61
35	Dual-Polarization GNSS-R Interference Pattern Technique for Soil Moisture Mapping. IEEE Journal of Selected Topics in Applied Earth Observations and Remote Sensing, 2014, 7, 1533-1544.	4.9	61
36	Angular resolution of two-dimensional, hexagonally sampled interferometric radiometers. Radio Science, 1998, 33, 1459-1473.	1.6	58

#	Article	IF	CITATIONS
37	Sea-State Determination Using GNSS-R Data. IEEE Geoscience and Remote Sensing Letters, 2010, 7, 621-625.	3.1	58
38	Optimization and Performance Analysis of Interferometric GNSS-R Altimeters: Application to the PARIS IoD Mission. IEEE Journal of Selected Topics in Applied Earth Observations and Remote Sensing, 2014, 7, 1436-1451.	4.9	58
39	Sea Target Detection Using Spaceborne GNSS-R Delay-Doppler Maps: Theory and Experimental Proof of Concept Using TDS-1 Data. IEEE Journal of Selected Topics in Applied Earth Observations and Remote Sensing, 2017, 10, 4237-4255.	4.9	58
40	Using DDM Asymmetry Metrics for Wind Direction Retrieval From GPS Ocean-Scattered Signals in Airborne Experiments. IEEE Transactions on Geoscience and Remote Sensing, 2014, 52, 3924-3936.	6.3	55
41	GNSS Transpolar Earth Reflectometry exploriNg System (G-TERN): Mission Concept. IEEE Access, 2018, 6, 13980-14018.	4.2	55
42	Extension of the Clean Technique to the Microwave Imaging of Continuous Thermal Sources by Means of Aperture Synthesis Radiometers. Progress in Electromagnetics Research, 1998, 18, 67-83.	4.4	53
43	Radio-Frequency Interference Detection and Mitigation Algorithms for Synthetic Aperture Radiometers. Algorithms, 2011, 4, 155-182.	2.1	51
44	Ocean Surface's Scattering Coefficient Retrieval by Delay–Doppler Map Inversion. IEEE Geoscience and Remote Sensing Letters, 2011, 8, 750-754.	3.1	50
45	Sun effects in 2-D aperture synthesis radiometry imaging and their cancelation. IEEE Transactions on Geoscience and Remote Sensing, 2004, 42, 1161-1167.	6.3	49
46	Improved MUSIC-Based SMOS RFI Source Detection and Geolocation Algorithm. IEEE Transactions on Geoscience and Remote Sensing, 2016, 54, 1311-1322.	6.3	49
47	A Spatially Consistent Downscaling Approach for SMOS Using an Adaptive Moving Window. IEEE Journal of Selected Topics in Applied Earth Observations and Remote Sensing, 2018, 11, 1883-1894.	4.9	49
48	Impact of antenna errors on the radiometric accuracy of large aperture synthesis radiometers. Radio Science, 1997, 32, 657-668.	1.6	48
49	Brightness-Temperature Retrieval Methods in Synthetic Aperture Radiometers. IEEE Transactions on Geoscience and Remote Sensing, 2009, 47, 285-294.	6.3	48
50	Vegetation Water Content Estimation Using GNSS Measurements. IEEE Geoscience and Remote Sensing Letters, 2012, 9, 282-286.	3.1	48
51	High Angular Resolution RFI Localization in Synthetic Aperture Interferometric Radiometers Using Direction-of-Arrival Estimation. IEEE Geoscience and Remote Sensing Letters, 2015, 12, 102-106.	3.1	48
52	3Cat-2—An Experimental Nanosatellite for GNSS-R Earth Observation: Mission Concept and Analysis. IEEE Journal of Selected Topics in Applied Earth Observations and Remote Sensing, 2016, 9, 4540-4551.	4.9	48
53	Normality Analysis for RFI Detection in Microwave Radiometry. Remote Sensing, 2010, 2, 191-210.	4.0	46
54	Design and First Results of an UAV-Borne L-Band Radiometer for Multiple Monitoring Purposes. Remote Sensing, 2010, 2, 1662-1679.	4.0	45

#	Article	IF	CITATIONS
55	Snow Thickness Monitoring Using GNSS Measurements. IEEE Geoscience and Remote Sensing Letters, 2012, 9, 1109-1113.	3.1	45
56	Impact of receiver errors on the radiometric resolution of large two-dimensional aperture synthesis radiometers. Radio Science, 1997, 32, 629-641.	1.6	44
57	Multi-Temporal Evaluation of Soil Moisture and Land Surface Temperature Dynamics Using in Situ and Satellite Observations. Remote Sensing, 2016, 8, 587.	4.0	44
58	First Polarimetric GNSS-R Measurements from a Stratospheric Flight over Boreal Forests. Remote Sensing, 2015, 7, 13120-13138.	4.0	43
59	Internet of Satellites (IoSat): Analysis of Network Models and Routing Protocol Requirements. IEEE Access, 2018, 6, 20390-20411.	4.2	43
60	The SMOS end-to-end performance simulator: description and scientific applications. , 0, , .		42
61	Predicting the Extent of Wildfires Using Remotely Sensed Soil Moisture and Temperature Trends. IEEE Journal of Selected Topics in Applied Earth Observations and Remote Sensing, 2016, 9, 2818-2829.	4.9	42
62	Polarimetric Formulation of the Visibility Function Equation Including Cross-Polar Antenna Patterns. IEEE Geoscience and Remote Sensing Letters, 2005, 2, 292-295.	3.1	41
63	Precision Bounds in GNSS-R Ocean Altimetry. IEEE Journal of Selected Topics in Applied Earth Observations and Remote Sensing, 2014, 7, 1416-1423.	4.9	41
64	First Results of a GNSS-R Experiment From a Stratospheric Balloon Over Boreal Forests. IEEE Transactions on Geoscience and Remote Sensing, 2016, 54, 2652-2663.	6.3	41
65	Sea surface emissivity observations at L-band: first results of the Wind and Salinity Experiment WISE 2000. IEEE Transactions on Geoscience and Remote Sensing, 2002, 40, 2117-2130.	6.3	40
66	Sensitivity of L-band vegetation optical depth to carbon stocks in tropical forests: a comparison to higher frequencies and optical indices. Remote Sensing of Environment, 2019, 232, 111303.	11.0	40
67	Wind speed effect on L-band brightness temperature inferred from EuroSTARRS and WISE 2001 field experiments. IEEE Transactions on Geoscience and Remote Sensing, 2004, 42, 2206-2213.	6.3	38
68	Spatial-Resolution Enhancement of SMOS Data: A Deconvolution-Based Approach. IEEE Transactions on Geoscience and Remote Sensing, 2009, 47, 2182-2192.	6.3	38
69	GNSS-R Derived Centimetric Sea Topography: An Airborne Experiment Demonstration. IEEE Journal of Selected Topics in Applied Earth Observations and Remote Sensing, 2013, 6, 1468-1478.	4.9	37
70	Analysis of noise-injection networks for interferometric-radiometer calibration. IEEE Transactions on Microwave Theory and Techniques, 2000, 48, 545-552.	4.6	36
71	L-band sea surface emissivity: Preliminary results of the WISE-2000 campaign and its application to salinity retrieval in the SMOS mission. Radio Science, 2003, 38, n/a-n/a.	1.6	36
72	On the Synergy of Airborne GNSS-R and Landsat 8 for Soil Moisture Estimation. Remote Sensing, 2015, 7, 9954-9974.	4.0	36

#	Article	IF	CITATIONS
73	Retrieving sea surface salinity with multiangular L-band brightness temperatures: Improvement by spatiotemporal averaging. Radio Science, 2005, 40, n/a-n/a.	1.6	35
74	Determination of sea surface salinity and wind speed by L-band microwave radiometry from a fixed platform. International Journal of Remote Sensing, 2004, 25, 111-128.	2.9	34
75	Performance of sea surface salinity and soil moisture retrieval algorithms with different auxiliary datasets in 2-D L-band aperture synthesis interferometric radiometers. IEEE Transactions on Geoscience and Remote Sensing, 2005, 43, 1189-1200.	6.3	34
76	Assessing LoRa for Satellite-to-Earth Communications Considering the Impact of Ionospheric Scintillation. IEEE Access, 2020, 8, 165570-165582.	4.2	34
77	Experimental Evaluation of GNSS-Reflectometry Altimetric Precision Using the P(Y) and C/A Signals. IEEE Journal of Selected Topics in Applied Earth Observations and Remote Sensing, 2014, 7, 1493-1500.	4.9	33
78	Ionospheric Effects in GNSS-Reflectometry From Space. IEEE Journal of Selected Topics in Applied Earth Observations and Remote Sensing, 2016, 9, 5851-5861.	4.9	33
79	Impact on Sea Surface Salinity Retrieval of Different Auxiliary Data Within the SMOS Mission. IEEE Transactions on Geoscience and Remote Sensing, 2006, 44, 2769-2778.	6.3	32
80	New Instrument Concepts for Ocean Sensing: Analysis of the PAU-Radiometer. IEEE Transactions on Geoscience and Remote Sensing, 2007, 45, 3180-3192.	6.3	32
81	Experimental Determination of the Sea Correlation Time Using GNSS-R Coherent Data. IEEE Geoscience and Remote Sensing Letters, 2010, 7, 675-679.	3.1	32
82	Mitigation of Direct Signal Cross-Talk and Study of the Coherent Component in GNSS-R. IEEE Geoscience and Remote Sensing Letters, 2015, 12, 279-283.	3.1	32
83	Denormalization of Visibilities for In-Orbit Calibration of Interferometric Radiometers. IEEE Transactions on Geoscience and Remote Sensing, 2006, 44, 2679-2686.	6.3	31
84	Cross-Correlation Waveform Analysis for Conventional and Interferometric GNSS-R Approaches. IEEE Journal of Selected Topics in Applied Earth Observations and Remote Sensing, 2014, 7, 1560-1572.	4.9	31
85	Automatic calibration of channels frequency response in interferometric radiometers. Electronics Letters, 1999, 35, 115.	1.0	30
86	On-Ground Characterization of the SMOS Payload. IEEE Transactions on Geoscience and Remote Sensing, 2009, 47, 3123-3133.	6.3	30
87	Radio Frequency Interference Detection and Mitigation Algorithms Based on Spectrogram Analysis. Algorithms, 2011, 4, 239-261.	2.1	30
88	Analysis of Spaceborne GNSS-R Delay-Doppler Tracking. IEEE Journal of Selected Topics in Applied Earth Observations and Remote Sensing, 2014, 7, 1481-1492.	4.9	30
89	Nodal Sampling: A New Image Reconstruction Algorithm for SMOS. IEEE Transactions on Geoscience and Remote Sensing, 2016, 54, 2314-2328.	6.3	30
90	Improving the Accuracy of Soil Moisture Retrievals Using the Phase Difference of the Dual-Polarization GNSS-R Interference Patterns. IEEE Geoscience and Remote Sensing Letters, 2014, 11, 2090-2094.	3.1	29

#	Article	IF	CITATIONS
91	Feasibility of precise navigation in high and low latitude regions under scintillation conditions. Journal of Space Weather and Space Climate, 2018, 8, A05.	3.3	29
92	Snow and Ice Thickness Retrievals Using GNSS-R: Preliminary Results of the MOSAiC Experiment. Remote Sensing, 2020, 12, 4038.	4.0	29
93	In-Orbit Validation of the FMPL-2 Instrument—The GNSS-R and L-Band Microwave Radiometer Payload of the FSSCat Mission. Remote Sensing, 2021, 13, 121.	4.0	29
94	Analysis of correlation and total power radiometer front-ends using noise waves. IEEE Transactions on Geoscience and Remote Sensing, 2005, 43, 2452-2459.	6.3	28
95	Impact of day/night time land surface temperature in soil moisture disaggregation algorithms. European Journal of Remote Sensing, 2016, 49, 899-916.	3.5	28
96	Assessment of Multi-Scale SMOS and SMAP Soil Moisture Products across the Iberian Peninsula. Remote Sensing, 2020, 12, 570.	4.0	28
97	Surface Topography and Mixed-Pixel Effects on the Simulated L-Band Brightness Temperatures. IEEE Transactions on Geoscience and Remote Sensing, 2007, 45, 1996-2003.	6.3	27
98	Fast Processing Tool for SMOS Data. , 2008, , .		27
99	End-to-end simulator for Global Navigation Satellite System Reflectometry space mission. , 2010, , .		27
100	Numerical Computation of the Electromagnetic Bias in GNSS-R Altimetry. IEEE Transactions on Geoscience and Remote Sensing, 2016, 54, 489-498.	6.3	27
101	Ceneric Performance Simulator of Spaceborne GNSS-Reflectometer for Land Applications. IEEE Journal of Selected Topics in Applied Earth Observations and Remote Sensing, 2020, 13, 3179-3191.	4.9	27
102	The Flexible Microwave Payload-2: A SDR-Based GNSS-Reflectometer and <i>L</i> -Band Radiometer for CubeSats. IEEE Journal of Selected Topics in Applied Earth Observations and Remote Sensing, 2020, 13, 1298-1311.	4.9	27
103	RFI Mitigation in Microwave Radiometry Using Wavelets. Algorithms, 2009, 2, 1248-1262.	2.1	26
104	Rfianalysis in smos imagery. , 2010, , .		26
105	Retracking considerations in spaceborne GNSS-R altimetry. GPS Solutions, 2012, 16, 507-518.	4.3	26
106	Delay Tracking in Spaceborne GNSS-R Ocean Altimetry. IEEE Geoscience and Remote Sensing Letters, 2013, 10, 57-61.	3.1	26
107	Fsscat, the 2017 Copernicus Masters' "Esa Sentinel Small Satellite Challenge―Winner: A Federated Polar and Soil Moisture Tandem Mission Based on 6U Cubesats. , 2018, , .		26
108	End-to-end simulator of two-dimensional interferometric radiometry. Radio Science, 2003, 38, n/a-n/a.	1.6	25

#	Article	IF	CITATIONS
109	Common Mathematical Framework for Real and Synthetic Aperture by Interferometry Radiometers. IEEE Transactions on Geoscience and Remote Sensing, 2014, 52, 38-50.	6.3	25
110	Benefits of Using Mobile Ad-Hoc Network Protocols in Federated Satellite Systems for Polar Satellite Missions. IEEE Access, 2018, 6, 56356-56367.	4.2	25
111	A Review of RFI Mitigation Techniques in Microwave Radiometry. Remote Sensing, 2019, 11, 3042.	4.0	25
112	SMOS REFLEX 2003: L-band emissivity characterization of vineyards. IEEE Transactions on Geoscience and Remote Sensing, 2005, 43, 973-982.	6.3	24
113	A Generic Level 1 Simulator for Spaceborne GNSS-R Missions and Application to GEROS-ISS Ocean Reflectometry. IEEE Journal of Selected Topics in Applied Earth Observations and Remote Sensing, 2017, 10, 4645-4659.	4.9	24
114	Single-Pass Soil Moisture Retrievals Using GNSS-R: Lessons Learned. Remote Sensing, 2020, 12, 2064.	4.0	24
115	AMIRAS—An Airborne MIRAS Demonstrator. IEEE Transactions on Geoscience and Remote Sensing, 2008, 46, 705-716.	6.3	23
116	Calibration of Correlation Radiometers Using Pseudo-Random Noise Signals. Sensors, 2009, 9, 6131-6149.	3.8	23
117	Characterization of the SMOS Instrumental Error Pattern Correction Over the Ocean. IEEE Geoscience and Remote Sensing Letters, 2012, 9, 793-797.	3.1	23
118	Advanced architectures for real-time Delay-Doppler Map GNSS-reflectometers: The GPS reflectometer instrument for PAU (griPAU). Advances in Space Research, 2010, 46, 196-207.	2.6	22
119	Determination of the Sea Surface Salinity Error Budget in the Soil Moisture and Ocean Salinity Mission. IEEE Transactions on Geoscience and Remote Sensing, 2010, 48, 1684-1693.	6.3	22
120	Improving the accuracy of sea surface salinity retrieval using GNSSâ€R data to correct the sea state effect. Radio Science, 2011, 46, .	1.6	22
121	PARIS Interferometric Technique proof of concept: Sea surface altimetry measurements. , 2012, , .		22
122	Modeling and Analysis of GNSS-R Waveforms Sample-to-Sample Correlation. IEEE Journal of Selected Topics in Applied Earth Observations and Remote Sensing, 2014, 7, 1545-1559.	4.9	22
123	Performance Assessment of Time–Frequency RFI Mitigation Techniques in Microwave Radiometry. IEEE Journal of Selected Topics in Applied Earth Observations and Remote Sensing, 2017, 10, 3096-3106.	4.9	22
124	The correlation of visibility noise and its impact on the radiometric resolution of an aperture synthesis radiometer. IEEE Transactions on Geoscience and Remote Sensing, 2000, 38, 2423-2426.	6.3	21
125	Noise maps in aperture synthesis radiometric images due to cross-correlation of visibility noise. Radio Science, 2003, 38, n/a-n/a.	1.6	21
126	The light airborne reflectometer for GNSS-R observations (LARGO) instrument: Initial results from airborne and Rover field campaigns. , 2014, , .		21

#	Article	IF	CITATIONS
127	SNR Degradation in GNSS-R Measurements Under the Effects of Radio-Frequency Interference. IEEE Journal of Selected Topics in Applied Earth Observations and Remote Sensing, 2016, 9, 4865-4878.	4.9	21
128	The Role of Climatic Anomalies and Soil Moisture in the Decline of Drought-Prone Forests. IEEE Journal of Selected Topics in Applied Earth Observations and Remote Sensing, 2017, 10, 503-514.	4.9	21
129	Single-Pass Soil Moisture Retrieval Using GNSS-R at L1 and L5 Bands: Results from Airborne Experiment. Remote Sensing, 2021, 13, 797.	4.0	21
130	Potential Synergetic Use of GNSS-R Signals to Improve the Sea-State Correction in the Sea Surface Salinity Estimation: Application to the SMOS Mission. IEEE Transactions on Geoscience and Remote Sensing, 2007, 45, 2088-2097.	6.3	20
131	Simulated SMOS Levels 2 and 3 Products: The Effect of Introducing ARGO Data in the Processing Chain and Its Impact on the Error Induced by the Vicinity of the Coast. IEEE Transactions on Geoscience and Remote Sensing, 2009, 47, 3041-3050.	6.3	20
132	Microwave Radiometer Resolution Optimization Using Variable Observation Times. Remote Sensing, 2010, 2, 1826-1843.	4.0	20
133	Surface moisture and temperature trends anticipate drought conditions linked to wildfire activity in the Iberian Peninsula. European Journal of Remote Sensing, 2016, 49, 955-971.	3.5	20
134	Mutual coupling effects on antenna radiation pattern: An experimental study applied to interferometric radiometers. Radio Science, 1998, 33, 1543-1552.	1.6	18
135	New radiometers: SMOS-a dual pol L-band 2D aperture synthesis radiometer. , 0, , .		18
136	On the Correlation Between GNSS-R Reflectivity and L-Band Microwave Radiometry. IEEE Journal of Selected Topics in Applied Earth Observations and Remote Sensing, 2016, 9, 5862-5879.	4.9	18
137	Improved characterization and modeling of equatorial plasma depletions. Journal of Space Weather and Space Climate, 2018, 8, A38.	3.3	18
138	Gaps Analysis and Requirements Specification for the Evolution of Copernicus System for Polar Regions Monitoring: Addressing the Challenges in the Horizon 2020–2030. Remote Sensing, 2018, 10, 1098.	4.0	18
139	Design and Optimization of a Polar Satellite Mission to Complement the Copernicus System. IEEE Access, 2018, 6, 34777-34789.	4.2	18
140	Oil slicks detection using GNSS-R. , 2011, , .		17
141	Simulation and Analysis of GNSS-R Composite Waveforms Using GPS and Galileo Signals. IEEE Journal of Selected Topics in Applied Earth Observations and Remote Sensing, 2014, 7, 1461-1468.	4.9	17
142	First Dual-Band Multiconstellation GNSS-R Scatterometry Experiment Over Boreal Forests From a Stratospheric Balloon. IEEE Journal of Selected Topics in Applied Earth Observations and Remote Sensing, 2016, 9, 4743-4751.	4.9	17
143	Soil Moisture Estimation Synergy Using GNSS-R and L-Band Microwave Radiometry Data from FSSCat/FMPL-2. Remote Sensing, 2021, 13, 994.	4.0	17
144	Calibration and experimental results of a two-dimensional interferometric radiometer laboratory prototype. Radio Science, 1997, 32, 1821-1832.	1.6	16

#	Article	IF	CITATIONS
145	Experimental relationship between the sea brightness temperature changes and the GNSS-R delay-Doppler maps: Preliminary results of the albatross field experiments. , 2009, , .		16
146	On the Use of GNSS-R Data to Correct L-Band Brightness Temperatures for Sea-State Effects: Results of the ALBATROSS Field Experiments. IEEE Transactions on Geoscience and Remote Sensing, 2011, 49, 3225-3235.	6.3	16
147	An imaging algorithm for synthetic aperture interferometric radiometers with built-in RFI mitigation. , 2014, , .		16
148	Unified GNSS-R formulation including coherent and incoherent scattering components. , 2016, , .		16
149	Wind Direction Signatures in GNSS-R Observables from Space. Remote Sensing, 2018, 10, 198.	4.0	16
150	Untangling the Incoherent and Coherent Scattering Components in GNSS-R and Novel Applications. Remote Sensing, 2020, 12, 1208.	4.0	16
151	Redundant space calibration of hexagonal and Y-shaped beamforming radars and interferometric radiometers. International Journal of Remote Sensing, 2003, 24, 5183-5196.	2.9	15
152	Sea state effect on the sea surface emissivity at l-band. IEEE Transactions on Geoscience and Remote Sensing, 2003, 41, 2307-2315.	6.3	15
153	Angular and Radiometric Resolution of Y-Shaped Nonuniform Synthetic Aperture Radiometers for Earth Observation. IEEE Geoscience and Remote Sensing Letters, 2008, 5, 793-795.	3.1	15
154	Sea surface salinity retrievals from HUT-2D L-band radiometric measurements. Remote Sensing of Environment, 2010, 114, 1756-1764.	11.0	15
155	A General Analysis of the Impact of Digitization in Microwave Correlation Radiometers. Sensors, 2011, 11, 6066-6087.	3.8	15
156	Real-Time RFI Detection and Mitigation System for Microwave Radiometers. IEEE Transactions on Geoscience and Remote Sensing, 2013, 51, 4928-4935.	6.3	15
157	DME/TACAN Impact Analysis on GNSS Reflectometry. IEEE Journal of Selected Topics in Applied Earth Observations and Remote Sensing, 2016, 9, 4611-4620.	4.9	15
158	Assessment of Satellite Contacts Using Predictive Algorithms for Autonomous Satellite Networks. IEEE Access, 2020, 8, 100732-100748.	4.2	15
159	L-Band Vegetation Optical Depth Estimation Using Transmitted GNSS Signals: Application to GNSS-Reflectometry and Positioning. Remote Sensing, 2020, 12, 2352.	4.0	15
160	Remote Sensing of Precipitation Using Reflected GNSS Signals: Response Analysis of Polarimetric Observations. IEEE Transactions on Geoscience and Remote Sensing, 2022, 60, 1-12.	6.3	15
161	Sea Ice Concentration and Sea Ice Extent Mapping with L-Band Microwave Radiometry and GNSS-R Data from the FFSCat Mission Using Neural Networks. Remote Sensing, 2021, 13, 1139.	4.0	15
162	Sea Surface Salinity and Wind Speed Retrievals Using GNSS-R and L-Band Microwave Radiometry Data from FMPL-2 Onboard the FSSCat Mission. Remote Sensing, 2021, 13, 3224.	4.0	15

#	Article	IF	CITATIONS
163	Threshold and timing errors of 1 bit/2 level digital correlators in Earth observation synthetic aperture radiometry. Electronics Letters, 1997, 33, 812.	1.0	14
164	Determination of the sea surface emissivity at Lâ€band and application to SMOS salinity retrieval algorithms: Review of the contributions of the UPCâ€ICM. Radio Science, 2008, 43, .	1.6	14
165	Soil moisture downscaling activities at the REMEDHUS Cal/Val site and its application to SMOS. , 2010, , .		14
166	Snow monitoring using GNSS-R techniques. , 2011, , .		14
167	Impact of Rain, Swell, and Surface Currents on the Electromagnetic Bias in GNSS-Reflectometry. IEEE Journal of Selected Topics in Applied Earth Observations and Remote Sensing, 2016, 9, 4643-4649.	4.9	14
168	GNSS-R Altimetry Performance Analysis for the GEROS Experiment on Board the International Space Station. Sensors, 2017, 17, 1583.	3.8	14
169	Satellite Cross-Talk Impact Analysis in Airborne Interferometric Global Navigation Satellite System-Reflectometry with the Microwave Interferometric Reflectometer. Remote Sensing, 2019, 11, 1120.	4.0	14
170	Nanosatellites and Applications to Commercial and Scientific Missions. , 0, , .		14
171	Architectures and Synchronization Techniques for Distributed Satellite Systems: A Survey. IEEE Access, 2022, 10, 45375-45409.	4.2	14
172	The impact of antenna pattern frequency dependence in aperture synthesis microwave radiometers. IEEE Transactions on Geoscience and Remote Sensing, 2005, 43, 2218-2224.	6.3	13
173	Towards a coherent sea surface salinity product from SMOS radiometric measurements and ARGO buoys. , 2007, , .		13
174	Assessment of the topography impact on microwave radiometry at Lâ€band. Journal of Geophysical Research, 2008, 113, .	3.3	13
175	On the use of compact L-band Dicke radiometer (ARIEL) and UAV for soil moisture and salinity map retrieval: 2008/2009 field experiments. , 2009, , .		13
176	Soil moisture and vegetation height retrieval using GNSS-R techniques. , 2009, , .		13
177	New approach to sea surface wind retrieval from GNSS-R measurements. , 2011, , .		13
178	Implementation of a GNSS-R Payload Based on Software-Defined Radio for the 3CAT-2 Mission. IEEE Journal of Selected Topics in Applied Earth Observations and Remote Sensing, 2016, 9, 4824-4833.	4.9	13
179	3Cat-4: Combined GNSS-R, L-Band Radiometer with RFI Mitigation, and AIS Receiver for a I-Unit Cubesat Based on Software Defined Radio. , 2018, , .		13
180	Analytical Computation of the Spatial Resolution in GNSS-R and Experimental Validation at L1 and L5. Remote Sensing, 2020, 12, 3910.	4.0	13

#	Article	IF	CITATIONS
181	A new space technology for ocean observation: the SMOS mission. Scientia Marina, 2012, 76, 249-259.	0.6	13
182	Dynamic range and linearity trade-off in detectors for interferometric radiometers. Electronics Letters, 2003, 39, 1852.	1.0	12
183	L-band dielectric properties of different soil types collected during the mouse 2004 field experiment. , 0, , .		12
184	PAU/GNSS-R: Implementation, Performance and First Results of a Real-Time Delay-Doppler Map Reflectometer Using Global Navigation Satellite System Signals. Sensors, 2008, 8, 3005-3019.	3.8	12
185	New Passive Instruments Developed for Ocean Monitoring at the Remote Sensing Lab—Universitat Politècnica de Catalunya. Sensors, 2009, 9, 10171-10189.	3.8	12
186	PAU instrument aboard INTA MicroSat-1: A GNSS-R demonstration mission for sea state correction in L-band radiometry. , 2011, , .		12
187	Detecting Targets above the Earth's Surface Using GNSS-R Delay Doppler Maps: Results from TDS-1. Remote Sensing, 2019, 11, 2327.	4.0	12
188	First Evidences of Ionospheric Plasma Depletions Observations Using GNSS-R Data from CYGNSS. Remote Sensing, 2020, 12, 3782.	4.0	12
189	The Potential of Spaceborne GNSS Reflectometry for Soil Moisture, Biomass, and Freeze–Thaw Monitoring: Summary of a European Space Agency-funded study. IEEE Geoscience and Remote Sensing Magazine, 2022, 10, 8-38.	9.6	12
190	FPGA-based Implementation of a DDM-generator for GPS-reflectometry. , 2006, , .		11
191	FPGA-based Implementation of a Polarimetric Radiometer with Digital Beamforming. , 2006, , .		11
192	Microwave Aperture Synthesis Radiometry: Paving the Path for Sea Surface Salinity Measurement from Space. , 2008, , 223-238.		11
193	Review of the CALIMAS Team Contributions to European Space Agency's Soil Moisture and Ocean Salinity Mission Calibration and Validation. Remote Sensing, 2012, 4, 1272-1309.	4.0	11
194	Hyperspectral Optical, Thermal, and Microwave L-Band Observations For Soil Moisture Retrieval at Very High Spatial Resolution. Photogrammetric Engineering and Remote Sensing, 2014, 80, 745-755.	0.6	11
195	Microwave Imaging Radiometers by Aperture Synthesis—Performance Simulator (Part 1): Radiative Transfer Module. Journal of Imaging, 2016, 2, 17.	3.0	11
196	Crosstalk Statistics and Impact in Interferometric GNSS-R. IEEE Journal of Selected Topics in Applied Earth Observations and Remote Sensing, 2016, 9, 4621-4630.	4.9	11
197	Strong RFI Impact Mitigation in the Synthetic Aperture Interferometric Radiometer. , 2018, , .		11
198	Experimental Evidence of Swell Signatures in Airborne L5/E5a GNSS-Reflectometry. Remote Sensing, 2020, 12, 1759.	4.0	11

#	Article	IF	CITATIONS
199	Sea Surface Salinity Retrieval from Space: Potential Synergetic Use of GNSS-R Signals to Improve the Sea State Correction and Application to the SMOS Mission. , 0, , .		10
200	Design of a Compact Dual-Polarization Receiver for Pseudo-Correlation Radiometers at L-band. , 2006, ,		10
201	Polarimetric Emission of Rain Events: Simulation and Experimental Results at X-Band. Remote Sensing, 2009, 1, 107-121.	4.0	10
202	Water level monitoring using the interference pattern GNSS-R technique. , 2011, , .		10
203	A downscaling approach to combine SMOS multi-angular and full-polarimetric observations with MODIS VIS/IR data into high resolution soil moisture maps. , 2012, , .		10
204	Empirical Results of a Surface-Level GNSS-R Experiment in a Wave Channel. Remote Sensing, 2015, 7, 7471-7493.	4.0	10
205	A CubeSAT payload for in-situ monitoring of pentacene degradation due to atomic oxygen etching in LEO. Acta Astronautica, 2016, 126, 456-462.	3.2	10
206	Towards Federated Satellite Systems and Internet of Satellites: The Federation Deployment Control Protocol. Remote Sensing, 2021, 13, 982.	4.0	10
207	Sea surface salinity retrieval using multi-angular L-band radiometry: numerical study using the SMOS End-to-end Performance Simulator. , 0, , .		9
208	Impact and compensation of diffuse sun scattering in 2D aperture synthesis radiometers imagery. , 0, , .		9
209	Considerations About Antenna Pattern Measurements of 2-D Aperture Synthesis Radiometers. IEEE Geoscience and Remote Sensing Letters, 2006, 3, 259-261.	3.1	9
210	Soil Moisture Retrieval Using L-band Radiometry: Dependence on Soil Type and Moisture Profiles. , 0, , .		9
211	Inter-Element Phase Calibration in Interferometric Radiometers. , 2006, , .		9
212	Synthetic Aperture PAU: a new instrument to test potential improvements for future SMOSops. , 2007, ,		9
213	Soil Moisture Retrieval Using GNSS-R Techniques: Measurement Campaign in a Wheat Field. , 2008, , .		9
214	PAU/RAD: Design and Preliminary Calibration Results of a New L-Band Pseudo-Correlation Radiometer Concept. Sensors, 2008, 8, 4392-4412.	3.8	9
215	PAU-SA: A Synthetic Aperture Interferometric Radiometer Test Bed for Potential Improvements in Future Missions. Sensors, 2012, 12, 7738-7777.	3.8	9
216	Experimental Study on the Performance of RFI Detection Algorithms in Microwave Radiometry: Toward an Optimum Combined Test. IEEE Transactions on Geoscience and Remote Sensing, 2013, 51, 4936-4944.	6.3	9

#	Article	IF	CITATIONS
217	Soil Moisture mapping using forward scattered GPS L1 signals. , 2013, , .		9
218	Assessment of back-end RFI mitigation techniques in passive remote sensing. , 2015, , .		9
219	The Global Navigation Satellite Systems Reflectometry (GNSS-R) Microwave Interferometric Reflectometer: Hardware, Calibration, and Validation Experiments. Sensors, 2019, 19, 1019.	3.8	9
220	Airborne GNSS-R: A Key Enabling Technology for Environmental Monitoring. IEEE Journal of Selected Topics in Applied Earth Observations and Remote Sensing, 2021, 14, 6652-6661.	4.9	9
221	<title>New calibration technique for interferometric radiometers</title> . , 1998, , .		9
222	FSSCat Mission Description and First Scientific Results of the FMPL-2 Onboard 3CAT-5/A. , 2021, , .		9
223	Extension of the Clean Technique To the Microwave Imaging of Continuous Thermal Sources By Means of Aperture Synthesis Radiometers - Abstract. Journal of Electromagnetic Waves and Applications, 1998, 12, 311-313.	1.6	8
224	Reliability analysis in aperture synthesis interferometric radiometers: Application toLband Microwave Imaging Radiometer with Aperture Synthesis instrument. Radio Science, 2001, 36, 107-117.	1.6	8
225	Sea surface emissivity at L-band: swell effects. , 0, , .		8
226	Sea foam effects on the brightness temperature at L-band. , 0, , .		8
227	PAU in SeoSAT: A Proposed Hybrid L-band Microwave Radiometer/GPS Reflectometer to Improve Sea Surface Salinity Estimates from Space. , 2008, , .		8
228	Radio Frequency Interference detection algorithm based on spectrogram analysis. , 2010, , .		8
229	The proof of concept for 3-cm Altimetry using the Paris Interferometric Technique. , 2010, , .		8
230	Interferometric GNSS-R achievable altimetric performance and compression/denoising using the wavelet transform: An experimental study. , 2012, , .		8
231	Improvement of the PAU/PARIS End-to-end Performance Simulator (P <sup>2</sup> EPS) in preparation for upcoming GNSS-R missions. , 2013, , .		8
232	Microwave Imaging Radiometers by Aperture Synthesis Performance Simulator (Part 2): Instrument Modeling, Calibration, and Image Reconstruction Algorithms. Journal of Imaging, 2016, 2, 18.	3.0	8
233	Ionospheric Scintillation Monitoring Using GNSS-R?. , 2018, , .		8
234	3Cat-3/MOTS Nanosatellite Mission for Optical Multispectral and GNSS-R Earth Observation: Concept and Analysis. Sensors, 2018, 18, 140.	3.8	8

#	Article	IF	CITATIONS
235	An Enhanced Resolution Brightness Temperature Product for Future Conical Scanning Microwave Radiometers. IEEE Transactions on Geoscience and Remote Sensing, 2022, 60, 1-12.	6.3	8
236	Ocean salinity observations with SMOS mission. , 0, , .		7
237	SMOS: a satellite mission to measure ocean surface salinity. , 2001, , .		7
238	New Radiometer Concepts for Ocean Remote Sensing: Description of the Passive Advanced Unit (PAU) for Ocean Monitoring. , 2006, , .		7
239	Ground-Based GNSS-R Measurements with the PAU Instrument and their Application to the Sea Surface Salinity Retrieval: First Results. , 2008, , .		7
240	The GPS and RAdiometric Joint Observations experiment at the REMEDHUS site (Zamora-Salamanca) Tj ETQq0 0	0 rgBT /O	verJock 10 Tf
241	Analysis of a Least-Squares Soil Moisture Retrieval Algorithm from L-band Passive Observations. Remote Sensing, 2010, 2, 352-374.	4.0	7
242	GNSS-R Delay-Doppler Maps over land: Preliminary results of the GRAJO field experiment. , 2010, , .		7
243	Impact of receiver's frequency response in GNSS reflectometers. , 2010, , .		7
244	Noise wave analysis of Dicke and noise injection radiometers: Complete S parameter analysis and effect of temperature gradients. Radio Science, 2010, 45, n/a-n/a.	1.6	7
245	Performance of soil moisture retrieval algorithms using multiangular L band brightness temperatures. Water Resources Research, 2010, 46, .	4.2	7
246	Description and Performance of an L-Band Radiometer with Digital Beamforming. Remote Sensing, 2011, 3, 14-40.	4.0	7
247	Impact of Doppler frequency compensation errors on spaceborne GNSS-R altimetry. , 2012, , .		7
248	Spatial patterns of SMOS downscaled soil moisture maps over the remedhus network (Spain). , 2012, , .		7
249	The microwave interferometric reflectometer. Part II: Back-end and processor descriptions. , 2014, , .		7
250	Improvement of PAU/PARIS end-to-end performance simulator (P <sup>2</sup> EPS): Land scattering including topography. , 2016, , .		7
251	<sup>3</sup> Cat-1 project: a multi-payload CubeSat for scientific experiments and technology demonstrators. European Journal of Remote Sensing, 2017, 50, 125-136.	3.5	7
252	A spatially consistent downscaling approach for SMOS using an adaptive moving window. , 2017, , .		7

#	Article	IF	CITATIONS
253	<sup>3</sup> Cat-4 Mission: A 1-Unit CubeSat for Earth Observation with a L-band Radiometer and a GNSS-Reflectometer Using Software Defined Radio. , 2019, , .		7
254	A Novel Dissemination Protocol to Deploy Opportunistic Services in Federated Satellite Systems. IEEE Access, 2020, 8, 142348-142365.	4.2	7
255	Uso de un modelo semi-empÃrico de emisividad del mar para la estimación aproximada de la salinidad superficial a partir de medidas realizadas con un radiómetro aerotransportado. Scientia Marina, 2008, 72, .	0.6	7
256	Evaluation of LoRa for Data Retrieval of Ocean Monitoring Sensors with LEO Satellites. , 2020, , .		7
257	A Preliminary Study on Ionospheric Scintillation Anomalies Detected Using GNSS-R Data from NASA CYGNSS Mission as Possible Earthquake Precursors. Remote Sensing, 2022, 14, 2555.	4.0	7
258	Experimental validation of radiometric sensitivity in correlation radiometers. Electronics Letters, 1998, 34, 2377.	1.0	6
259	Full polarimetric emissivity of vegetation-covered soils: vegetation structure effects. , 0, , .		6
260	A radar course at undergraduate level: an approach to systems engineering. IEEE Transactions on Education, 2003, 46, 497-501.	2.4	6
261	A 3 GPS-channels Doppler-delay receiver for remote sensing applications. , 0, , .		6
262	Study of maize plants effects in the retrieval of soil moisture using the interference pattern GNSS-R technique. , 2010, , .		6
263	The Microwave Interferometric Reflectometer. Part I: Front-end and beamforming description. , 2014, , .		6
264	Ice thickness effects on Aquarius brightness temperatures over Antarctica. Journal of Geophysical Research: Oceans, 2015, 120, 2856-2868.	2.6	6
265	Time-domain Statistics of the Electromagnetic Bias in GNSS-Reflectometry. Remote Sensing, 2015, 7, 11151-11162.	4.0	6
266	Microwave Radiometry. , 2017, , 131-290.		6
267	SNR and Standard Deviation of cGNSS-R and iGNSS-R Scatterometric Measurements. Sensors, 2017, 17, 183.	3.8	6
268	Selection of the Key Earth Observation Sensors and Platforms Focusing on Applications for Polar Regions in the Scope of Copernicus System 2020–2030. Remote Sensing, 2019, 11, 175.	4.0	6
269	Proof-of-Concept of a Federated Satellite System Between Two 6-Unit CubeSats for Distributed Earth Observation Satellite Systems. , 2019, , .		6
270	Phase and Baseline Calibration for Microwave Interferometric Radiometers Using Beacons. IEEE Transactions on Geoscience and Remote Sensing, 2020, 58, 5242-5253.	6.3	6

#	Article	IF	CITATIONS
271	Sea Ice Thickness Estimation Based on Regression Neural Networks Using L-Band Microwave Radiometry Data from the FSSCat Mission. Remote Sensing, 2021, 13, 1366.	4.0	6
272	Possible Evidence of Earthquake Precursors Observed in Ionospheric Scintillation Events Observed from Spaceborne GNSS-R Data. , 2021, , .		6
273	On-Demand Satellite Payload Execution Strategy for Natural Disasters Monitoring Using LoRa: Observation Requirements and Optimum Medium Access Layer Mechanisms. Remote Sensing, 2021, 13, 4014.	4.0	6
274	Design of a Deployable Helix Antenna at L-Band for a 1-Unit CubeSat: From Theoretical Analysis to Flight Model Results. Sensors, 2022, 22, 3633.	3.8	6
275	Optimum redundant array configurations for Earth observation aperture synthesis microwave radiometers. Electronics Letters, 2002, 38, 1205.	1.0	5
276	Inter-comparison study of asymptotic models for sea surface emissivity simulation at L-band. , 0, , .		5
277	Time-dependent sea surface numerical generation for remote sensing applications. , 0, , .		5
278	Soil moisture retrieval errors using l-band radiometry induced by the soil type variability. , 0, , .		5
279	Surface Topography and Mixed Pixel Effects on the Simulated L-band Brightness Temperatures. , 0, , .		5
280	Deconvolution algorithms in image reconstruction for aperture synthesis radiometers. , 2007, , .		5
281	PAU-CNSS/R, a real-time GPS-reflectometer for earth observation applications: architecture insights and preliminary results. , 2007, , .		5
282	Radiometric Resolution of Motion-Induced Synthetic Aperture Radiometer. IEEE Geoscience and Remote Sensing Letters, 2011, 8, 715-719.	3.1	5
283	Pycaro's instrument proof of concept. , 2012, , .		5
284	Comparison of GPS L1 and Galileo E1 signals for GNSS-R ocean altimetry. , 2013, , .		5
285	Accurate geolocation of rfi sources in smos imagery based on superresolution algorithms. , 2014, , .		5
286	Advances in the MIR instrument: Integration, control subsystem and analysis of the flight dynamics for beamsteering purposes. , 2015, , .		5
287	Optimized model-based design space exploration of distributed multi-orbit multi-platform Earth observation spacecraft architectures. , 2018, , .		5
288	Impact of Signal Quantization on the Performance of RFI Mitigation Algorithms. Remote Sensing, 2019, 11, 2023.	4.0	5

#	Article	IF	CITATIONS
289	Analyzing Spatio-Temporal Factors to Estimate the Response Time between SMOS and In-Situ Soil Moisture at Different Depths. Remote Sensing, 2020, 12, 2614.	4.0	5
290	Advanced GNSS-R Signals Processing With GPUs. IEEE Journal of Selected Topics in Applied Earth Observations and Remote Sensing, 2020, 13, 1158-1163.	4.9	5
291	Design and Testing of a Helix Antenna Deployment System for a 1U CubeSat. IEEE Access, 2021, 9, 66103-66114.	4.2	5
292	Integration of MIRAS breadboard and future activities. , 0, , .		5
293	Validation of SMOS L3 AND L4 Soil Moisture Products In The Remedhus (SPAIN) AND CEMADEN (BRAZIL) Networks. Revista Brasileira De Geografia Fisica, 2020, 13, 691-712.	0.1	5
294	On the Trade-Off Between Enhancement of the Spatial Resolution and Noise Amplification in Conical-Scanning Microwave Radiometers. IEEE Transactions on Geoscience and Remote Sensing, 2022, 60, 1-14.	6.3	5
295	Corrections To "Radiometric Sensitivity Computation In Aperture Synthesis Interferometric Radiometry". IEEE Transactions on Geoscience and Remote Sensing, 1998, 36, 1835-1835.	6.3	4
296	Sea surface emissivity observations at L-band: first preliminary results of the WInd and Salinity Experiment WISE-2000. , 0, , .		4
297	Emissivity of the sea surface roughened by rain: simulation results. , 0, , .		4
298	L-band sea surface emissivity radiometric observations under high winds: Preliminary results of the Wind and Salinity Experiment WISE-2001. , 0, , .		4
299	MIRAS imaging validation. , 0, , .		4
300	Three-antenna two-dimensional imaging correlation radiometer: concept and preliminary results. , 0, ,		4
301	Sea surface brightness temperature at L-band: impact of surface currents. , 0, , .		4
302	Baseline calibration of interferometric radiometers: experimental results. , 0, , .		4
303	Design and test of the L-band automatic radiometer (LAURA) temperature control. , 0, , .		4
304	Improved Image Reconstruction Algorithms for Aperture Synthesis Radiometers. , 2006, , .		4
305	Roughness Effects on the L-band Emission of Bare Soils: The T-REX Field Experiment. , 2006, , .		4
306	MIRAS-SMOS Demonstrator Test Campaigns at Polytechnic University of Catalonia. , 2006, , .		4

#	Article	IF	CITATIONS
307	Topography effects on the L-band emissivity of soils: TuRTLE 2006 field experiment. , 2007, , .		4
308	Some results of the MIRAS-SMOS demonstrator campaigns. , 2007, , .		4
309	Initials Results of the Passive Advanced Unit - Synthetic Aperture (PAU-SA). , 2008, , .		4
310	Extended Ocean Salinity Error Budget Analysis within the SMOS Mission. , 2008, , .		4
311	Numerical Simulation of the Full-Polarimetric Emissivity of Vines and Comparison with Experimental Data. Remote Sensing, 2009, 1, 300-317.	4.0	4
312	Multifrequency experimental radiometer with interference tracking for experiments over land and littoral: Meritxell. , 2009, , .		4
313	Digital beamforming analysis and performance for a digital L-band Pseudo-correlation radiometer. , 2009, , .		4
314	SMOS measurements preliminary validation against modeled brightness temperatures and external-source salinity data. , 2010, , .		4
315	Hardware implementation of a wavelet-based radio frequency interference mitigation algorithm for microwave radiometers. , 2011, , .		4
316	Experimental study of radio-frequency interference detection algorithms in microwave radiometry. , 2011, , .		4
317	Calibration, Performance, and Imaging Tests of a Fully Digital Synthetic Aperture Interferometer Radiometer. IEEE Journal of Selected Topics in Applied Earth Observations and Remote Sensing, 2012, 5, 723-734.	4.9	4
318	MIR: The microwave interferometric reflectometer, a new airborne sensor for GNSS-R advanced research. , 2013, , .		4
319	Temperature gradient sensor from pulsed power supply duty cycle in ultraâ€lowâ€power energy harvesting system. Electronics Letters, 2014, 50, 826-828.	1.0	4
320	A simulator for GNSS-R polarimetric observations over the ocean. , 2014, , .		4
321	Can we measure vegetation water content and vegetation opacity at L-band with a single GPS receiver?. , 2016, , .		4
322	Architectures and Synchronization Techniques for Coherent Distributed Remote Sensing Systems. , 2019, , .		4
323	Correcting the ADCS Jitter Induced Blurring in Small Satellite Imagery. IEEE Journal on Miniaturization for Air and Space Systems, 2020, 1, 130-137.	2.7	4
324	Deployment mechanism for a L-band helix antenna in 1-Unit Cubesat. Acta Astronautica, 2022, 196, 394-399.	3.2	4

#	Article	IF	CITATIONS
325	Implementation of a Testbed for GNSS-R Payload Performance Evaluation. IEEE Journal of Selected Topics in Applied Earth Observations and Remote Sensing, 2020, 13, 2708-2715.	4.9	4
326	A Novel RFI Detection Method for Microwave Radiometers Using Multilag Correlators. IEEE Transactions on Geoscience and Remote Sensing, 2022, 60, 1-12.	6.3	4
327	Bayesian Unsupervised Machine Learning Approach to Segment Arctic Sea Ice Using SMOS Data. Geophysical Research Letters, 2021, 48, e2020GL091285.	4.0	4
328	From Monolithic Satellites to the Internet of Satellites Paradigm: When Space, Air, and Ground Networks Become Interconnected. , 0, , .		4
329	Measurements and simulations of a doppler radiometer in an anechoic chamber. , 0, , .		3
330	Extension of Kirchhoff method under stationary phase approximation to determination of polarimetric thermal emission of the sea. Electronics Letters, 1998, 34, 1501.	1.0	3
331	Specification of channel filters for an interferometric radiometer. Radio Science, 2001, 36, 97-106.	1.6	3
332	The EuroSTARRS campaign in support of the Soil Moisture and Ocean Salinity mission. , 0, , .		3
333	SMOS performance simulation analysis. , 0, , .		3
334	Passive polarimetric remote sensing of the ocean surface during the Rough Evaporation Duct experiment (RED 2001). , 0, , .		3
335	From the Determination of Sea Emissivity to the Retrieval of Salinity: Recent Contributions to the SMOS Mission from the UPC and ICM. , 2006, , .		3
336	Correction to "A Two-Dimensional Doppler Radiometer for Earth Observation― IEEE Transactions on Geoscience and Remote Sensing, 2007, 45, 4194-4194.	6.3	3
337	Towards an ocean salinity error budget estimation within the SMOS mission. , 2007, , .		3
338	Empirical determination of the soil emissivity at L-band: Effects of soil moisture, soil roughness, vine canopy, and topography. , 2007, , .		3
339	Initial Results of an Airborne Light-Weight L-Band Radiometer. , 2008, , .		3
340	Image Reconstruction Algorithms for 2D Aperture Synthesis Radiometers. , 2008, , .		3
341	Use of Pseudo-Random Noise sequences in microwave radiometer calibration. , 2008, , .		3
342	Topographic profile retrieval using the Interference Pattern GNSS-R technique. , 2009, , .		3

Topographic profile retrieval using the Interference Pattern GNSS-R technique. , 2009, , . 342

20

#	Article	IF	CITATIONS
343	On-ground tests and measurements of the Passive Advanced Unit Synthetic Aperture (PAU-SA). , 2010, , .		3
344	SMOS' brightness temperatures validation: First results after the commisioning phase. , 2010, , .		3
345	Brightness temperature correction of the sea state effect using GNSS-R data. , 2010, , .		3
346	Airborne soil moisture determination using a data fusion approach at regional level. , 2011, , .		3
347	Airborne wind retrieval using GPS delay-Doppler maps. , 2012, , .		3
348	PAU Instrument aboard INTA MicroSAT-1: Initial results of the FM model from an airborne experiment. , 2012, , .		3
349	Recent advances in land monitoring using GNSS-R techniques. , 2012, , .		3
350	Land monitoring using GNSS-R techniques: A review of recent advances. , 2013, , .		3
351	On the synergy of SMOS and Terra/Aqua MODIS: High resolution soil moisture maps in near real-time. , 2013, , .		3
352	Study of RFI signals in protected GNSS bands generated by common electronic devices: Effects on GNSS-R measurements. , 2014, , .		3
353	Typhoon observations using the interferometric GNSS-R technique. , 2014, , .		3
354	An airborne GNSS-R field experiment over a vineyard for soil moisture estimation and monitoring. , 2015, , .		3
355	Geolocalizing SMOS RFI sources on the densely populated East Asia. , 2015, , .		3
356	Spaceborne GNSS-R End-To-End Simulator: Topography and Vegetation Effects. , 2018, , .		3
357	The Flexible Microwave Payload -2: Architecture and Testing of a Combined GNSS-R and L-Band Radiometer With RFI Mitigation Payload For Cubesat-Based Earth Observation Missions. , 2019, , .		3
358	Mission and system architecture for an operational network of earth observation satellite nodes. Acta Astronautica, 2020, 176, 398-412.	3.2	3
359	A Remote Carrier Synchronization Technique for Coherent Distributed Remote Sensing Systems. IEEE Journal of Selected Topics in Applied Earth Observations and Remote Sensing, 2021, 14, 1909-1922.	4.9	3
360	Improved GNSS-R Altimetry Methods: Theory and Experimental Demonstration Using Airborne Dual Frequency Data from the Microwave Interferometric Reflectometer (MIR). Remote Sensing, 2021, 13, 4186.	4.0	3

#	Article	IF	CITATIONS
361	Vegetation Canopy Height Retrieval Using L1 and L5 Airborne GNSS-R. IEEE Geoscience and Remote Sensing Letters, 2022, 19, 1-5.	3.1	3
362	On the Potential of Empirical Mode Decomposition for RFI Mitigation in Microwave Radiometry. IEEE Transactions on Geoscience and Remote Sensing, 2022, 60, 1-10.	6.3	3
363	<title>Evaluation of MIRAS spaceborne instrument performance: snapshot radiometric accuracy and its improvement by means of pixel averaging</title> . , 1997, , .		2
364	Remote sensing of hydrometeors by means of interferometric radiometry: Theory and experimental results. Radio Science, 2000, 35, 799-812.	1.6	2
365	SMOS radiometric performance evaluation using SEPS: evaluation of thermal drifts. , 0, , .		2
366	Impact on sea surface salinity retrieval of multi-source auxiliary data within the SMOS mission. , 0, , .		2
367	MIRAS In-Orbit Calibration. , 2007, , .		2
368	Calibration and performance analysis of the PAU- RAD instrument. , 2007, , .		2
369	Sea surface temperature retrieval using ir-radiometry and atmospheric modeling: Simulation and experimental results using PAU-IR. , 2007, , .		2
370	K-band radiometer designed for academic purposes: Intercomparison of performances as total power, dicke or noise injection radiometers. , 2007, , .		2
371	Radiometric observations of vines from the green period to the withering. , 2008, , .		2
372	Altimetry study performed using an airborne GNSS-Reflectometer. , 2010, , .		2
373	Impact of the observation geometry on the GNSS-R direct descriptors used for sea state monitoring. , 2012, , .		2
374	Cubesat-based demonstrator for optical earth observation. , 2012, , .		2
375	Height precision prediction of the PARIS in orbit demonstrator based on Cramer-Rao bound analysis. , 2012, , .		2
376	Submeter ocean altimetry with GPS L1 C/A signal. , 2012, , .		2
377	A generic simulator for aperture synthesis radiometers. , 2012, , .		2
378	PAU instrument aboard INTA MicroSat-1: Flight model tests. , 2012, , .		2

#	Article	IF	CITATIONS
379	Analysis of GNSS-R delay and Doppler tracking errors. , 2012, , .		2
380	Wind speed maping from the ISS using GNSS-R? A simulation study. , 2013, , .		2
381	Foreword to the Special Issue on Radio Frequency Interference: Identification, Mitigation, and Impact Assessment. IEEE Transactions on Geoscience and Remote Sensing, 2013, 51, 4915-4917.	6.3	2
382	Airborne GNSS-R, thermal and optical data relationships for soil moisture retrievals. , 2015, , .		2
383	Comparison of real-time time-frequency RFI mitigation techniques in microwave radiometry. , 2016, , .		2
384	MERITXELL: The Multifrequency Experimental Radiometer with Interference Tracking for Experiments over Land and Littoral—Instrument Description, Calibration and Performance. Sensors, 2017, 17, 1081.	3.8	2
385	Calibration of GNSS-R receivers with PRN signal injection: Methodology and validation with the microwave interferometric reflectometer (MIR). , 2017, , .		2
386	Preliminary Altimetry Results of the Malygnss Instrument in the Humit Project. , 2018, , .		2
387	Phase and Amplitude Calibrations of Rotating Equispaced Circular Array for Geostationary Microwave Interferometric Radiometers— Theory and Methods. IEEE Transactions on Geoscience and Remote Sensing, 2022, 60, 1-15.	6.3	2
388	In-Orbit Validation of the FMPL-2 Dual Microwave Payload Onboard the Fsscat Mission. , 2021, , .		2
389	Untangling the GNSS-R Coherent and Incoherent Components: Experimental Evidences Over the Ocean. , 2020, , .		2
390	Orbit Design for a Satellite Swarm-Based Motion Induced Synthetic Aperture Radiometer (MISAR) in Low-Earth Orbit for Earth Observation Applications. IEEE Transactions on Geoscience and Remote Sensing, 2022, 60, 1-16.	6.3	2
391	Impact of Incidence Angle Diversity on SMOS and Sentinel-1 Soil Moisture Retrievals at Coarse and Fine Scales. IEEE Transactions on Geoscience and Remote Sensing, 2022, 60, 1-18.	6.3	2
392	<title>Receiver specifications of the MIRAS demonstrator</title> ., 2001, 4169, 291.		1
393	Polarimetric emissivity of vegetation-covered soils: simulation results. , 0, , .		1
394	Sea surface emissivity at L-band: results of the WInd and Salinity Experiments WISE 2000 and 2001 and preliminary results from FROG 2003. , 2004, , .		1
395	External calibration in L-band 2D synthetic aperture radiometers: application to sea surface salinity retrieval. , 0, , .		1
396	Denormalization of visibilities for in-orbit calibration of interferometric radiometers. , 0, , .		1

Denormalization of visibilities for in-orbit calibration of interferometric radiometers. , 0, , . 396

#	Article	IF	CITATIONS
397	Retrieved Sea Surface Salinity Dependence on Multisource Auxiliary Data within the SMOS mission. , 0, , .		1
398	PAU one-receiver ground-based and airbone instruments. , 2007, , .		1
399	The impact of the number of bits in digital beamforming real aperture and synthetic aperture radiometers. , 2008, , .		1
400	MIRAS ground characterization. , 2008, , .		1
401	Rock Fraction Effects on the Surface Soil Moisture Estimates From L-Band Radiometric Measurements. , 2008, , .		1
402	Spatial Resolution Enhancement of SMOS Data: A Combined Fourier Wavelet Approach. , 2008, , .		1
403	Brightness Temperature Retrievals from the Small Airborne MIRAS. , 2008, , .		1
404	L-Band Radiometric Observations of Sun Clint Over Land Surfaces. , 2008, , .		1
405	Contributions to the Improvement of the SMOS Level 2 Retrieval Algorithm: Optimization of the Cost Function. , 2008, , .		1
406	Preliminary results of the Passive Advanced Unit Synthetic Aperture (PAU-SA). , 2009, , .		1
407	Preliminary results of the advanced L-band transmission and reflection observationof the sea surface (ALBATROSS) campaign: Preparing the SMOS calibration and validation activities. , 2009, , .		1
408	On-flight characterization of the SMOS payload during the commissioning phase. , 2009, , .		1
409	Normality analysis as a radio frequency interference detection. , 2010, , .		1
410	First results of the PAU-SA synthetic aperture radiometer. , 2011, , .		1
411	Preliminary error budget of a GNSS-R spaceborne mission. , 2011, , .		1
412	Error Covariance Matrices Characterization in the Ocean Salinity Retrieval Cost Function within the SMOS Mission. Journal of Atmospheric and Oceanic Technology, 2011, 28, 1155-1166.	1.3	1
413	Study of radio frequency interference effects on radiometry bands in urban environments. , 2012, , .		1
414	Validation and experimental tests of the PAU-synthetic aperture radiometer. , 2012, , .		1

#	Article	IF	CITATIONS
415	Digital back-end for RFI detection and mitigation in microwave radiometers. , 2012, , .		1
416	Optimum Intercalibration Time in Synthetic Aperture Interferometric Radiometers: Application to SMOS. IEEE Geoscience and Remote Sensing Letters, 2012, 9, 774-777.	3.1	1
417	SMOS CP34 soil moisture and ocean salinity maps. , 2012, , .		1
418	SMOS L3 salinity performances at decreasing sea surface temperature. , 2012, , .		1
419	SAIRPS: A generic simulator for evaluation of synthetic aperture interferometric radiometers. , 2013, , .		1
420	An IBC solar cell for the UPC CubeSat-1 mission. , 2013, , .		1
421	Digital back-end for RFI detection and mitigation in earth observation. , 2013, , .		1
422	Hyperspectral-derived indices for soil moisture estimation at very high resolution. , 2014, , .		1
423	Impact of the elevation angle in the coherence time as a function of the sea wave height. , 2015, , .		1
424	First Delay Doppler Maps obtained with the Microwave Inteferometric Reflectometer (MIR). , 2016, , .		1
425	Feasibility of RFI mitigation in synthetic aperture radiometery based on subspace spatial filtering. , 2017, , .		1
426	Microwave and Optical Data Fusion for Global Mapping of Soil Moisture at High Resolution. , 2018, , .		1
427	RFI Analysis and Mitigation in Airborne GNSS-R Campaign. , 2018, , .		1
428	Determination of Sea Correlation Time at L-Band with Airborne Reflected New GNSS Signals. , 2018, , .		1
429	Influence of Quality Filtering Approaches in BEC SMOS L3 Soil Moisture Products. , 2019, , .		1
430	An FFT-Based CLEAN Deconvolution Method for Interferometric Microwave Radiometers With Spatially Variable Beam Pattern. IEEE Geoscience and Remote Sensing Letters, 2021, 18, 341-345.	3.1	1
431	A Pre-Correlation RFI Mitigation Algorithm for L-Band Interferometric Radiometers. , 2021, , .		1
432	Soil Moisture Retrieval Using the FMPL-2/FSSCat GNSS-R and Microwave Radiometry Data. , 2021, , .		1

#	Article	IF	CITATIONS
433	Incidence Angle Diversity on L-Band Microwave Radiometry and Its Impact on Consistent Soil Moisture Retrievals. , 2021, , .		1
434	A Cubesat-Ready Phase Synchronization Digital Payload for Coherent Distributed Remote Sensing Missions. , 2021, , .		1
435	Sea Ice Concentration and Sea Ice Extent Mapping with the Fsscat Mission: A Neural Network Approach. , 2021, , .		1
436	Radio-Frequency Interference Location, Detection and Classification Using Deep Neural Networks. , 2020, , .		1
437	Demonstration of the Federated Satellite Systems Concept for Future Earth Observation Satellite Missions. , 2020, , .		1
438	<title>Millimeter-wave aperture synthesis for remote sensing of the Earth</title> ., 1998, 3498, 82.		0
439	<title>Modeling the radiometric signatures of the Earth from space: a tool to study the performance&lt;br&gt;of new radiometers</title> . , 1998, 3498, 484.		Ο
440	<title>WISE 2000 campaign: sea surface salinity and wind retrievals from L-band radiometry</title> . , 2000, 4172, 65.		0
441	Sea state influence on L-band emissivity in various fetch conditions. , 0, , .		Ο
442	Soil moisture retrieval by SMOS: a global feasibility study. , 0, , .		0
443	Errors on the retrieved sea surface salinity from microwave radiometry due to inaccuracies in the ancillary data. , 0, , .		Ο
444	Estimation of sea surface spectrum under non-stationary conditions. , 0, , .		0
445	Systematic noise analysis of a correlation radiometer front-end. , 0, , .		Ο
446	Estimation of sea surface spectrum using neural networks. , 2004, , .		0
447	Study of soil moisture retrieval algorithms using multiangular L-band brightness temperatures: application to ESA's SMOS Earth Explorer Opportunity Mission. , 2004, 5232, 596.		Ο
448	Retrieved sea surface salinity spatial variability using high resolution data within the soil moisture and ocean salinity (SMOS) mission. , 2007, , .		0
449	PAU-RAD instrument web-based remote control. , 2007, , .		0
450	The impact of combining SMOS and ARGO data on the SMOS Level 2 and 3 products and effect of the vicinity of the coast. , 2008, , .		0

#	Article	IF	CITATIONS
451	Initial Results of a Digital Radiometer with Digital Beamforming. , 2008, , .		0
452	Improving the Spatial Resolution of Synthetic Aperture Radiometer Imagery using Auxiliary Information: Application to the Smos Mission. , 2008, , .		0
453	Foreword to the Special Issue on the 2007 International Geoscience and Remote Sensing Symposium (IGARSS'07). IEEE Transactions on Geoscience and Remote Sensing, 2008, 46, 2767-2768.	6.3	Ο
454	Meridional variability in SMOS salinity retrievals: Trade-off between sensitivity to geophysical effects and increased temporal sampling. , 2009, , .		0
455	Noise wave analysis of Dicke and noise injection radiometers: Complete S-paramater analysis and effect of temperature gradients. , 2009, , .		0
456	Preparatory activities at the remedhus SMOS cal/val site: Characterisation of bare soils and effect of surface roughness. , 2010, , .		0
457	A radiometer concept to retrieve the 3-D radiometric emission from atmospheric temperature and water vapor density. , 2011, , .		Ο
458	Enhancing the spatial resolution of SMOS soil moisture data over Spain. , 2011, , .		0
459	Cross-correlation waveform mode: A critical review. , 2012, , .		Ο
460	Preliminary performance study of different radio-frequency interference detection and mitigation algorithms in microwave radiometry. , 2012, , .		0
461	GNSS-R altimeter performance: Analysis of Cramer-Rao lower bounds. , 2012, , .		Ο
462	Altimetry performance and error budget of the PARIS in-orbit demonstration mission. , 2013, , .		0
463	Ocean surface wind vector measurements from high-altitude aircraft using GPS delay-doppler maps. , 2013, , .		0
464	The dual polarization GNSS-R interference pattern technique. , 2014, , .		0
465	Review of GNSS-R instruments and tools developed at the Universitat Politecnica de Catalunya-Barcelona tech. , 2014, , .		0
466	A generic simulator for aperture synthesis radiometers: Radiative transfer module and end-to-end tests. , 2014, , .		0
467	3CAT-3/MOTS, an Experimental Nanosatellite for Multispectral and GNSS-R Earth Observation: Airborne Optical and GNSS-R Campaign. , 2018, , .		0
468	Hurricane Observations with GNSS-Reflectometry from CYGNSS Mission – Case Study of Hurricane Irma 2017. , 2019, , .		0

#	Article	IF	CITATIONS
469	Architecting Optimized Spaceborne Earth Observation Missions. , 2019, , .		0
470	Analyzing Anomalous Artefacts in TDS-1 Delay Doppler Maps. , 2019, , .		0
471	Quantization and Sampling Effects on Microwave Radiometry RFI Mitigation Algorithms. , 2019, , .		Ο
472	Phase and Amplitude Calibration of Rotating Equispaced Circular Array for Geostationary Microwave Interferometric Radiometers—Simulation Results and Discussion. IEEE Transactions on Geoscience and Remote Sensing, 2022, 60, 1-19.	6.3	0
473	Addendum: Hu, C.; et al. Detecting Targets above the Earth's Surface Using GNSS-R Delay Doppler Maps: Results from TDS-1. Remote Sens. 2019, 11, 2327. Remote Sensing, 2021, 13, 715.	4.0	0
474	Parameter Considerations for the Retrieval of Surface Soil Moisture from Spaceborne GNSS-R. , 2021, , .		0
475	Monitoring Forest Above-Ground Biomass from Multifrequency Vegetation Optical Depth: A Preliminary Study. , 2021, , .		0
476	Analysis on the Feasability of Airborne GNSS-R Receivers for Weather Nowcasting and Target Detection. , 2020, , .		0
477	FFSCAT Mission: Preliminary Results and Ice Products Validation with Mosaic Campaign Data. , 2020, , .		Ο
478	The GRSS Standard for GNSS-Reflectometry. , 2020, , .		0
479	First Experimental Evidence of Wind and Swell Signatures in L5 GPS and E5A Galileo GNSS-R Waveforms. , 2020, , .		Ο